Energy and Climate Change 1 (2020) 100008

Contents lists available at ScienceDirect

Energy and Climate Change

journal homepage: www.elsevier.com/locate/egycc

Full Length Article

Numerical simulation of building wall incorporating phase change material for cooling load reduction

K. Kant[a,b,*], A. Shukla[b], Atul Sharma[b]

[a] Department of Mechanical Engineering, Eindhoven University of Technology, 5600 MBEindhoven, the Netherlands
[b] Non-Conventional Energy Laboratory, Rajiv Gandhi Institute of Petroleum Technology, Jais Amethi 229304, India

ARTICLE INFO

Keywords:
PCM
Thermal energy storage
Energy efficiency
Indoor comfort

ABSTRACT

Phase change material (PCM) placed in the building wall changes the temperature profile within the wall and thus influences the heat transport to indoor environment. The effectiveness of these building walls depends on PCM location within the wall, PCM melting temperature, and PCM layer thickness. Considering these parameters, the numerical simulation has been conducted for a typical building wall and the obtained results are reported in terms of melt fraction of PCM and heat flux at the inner surface of the wall. From these results it is found that for the minimum heat transport to the indoor environment, the PCM layer should be embedded in between the fiberglass insulation layers, melting temperature of PCM should be in the range of indoor air temperature and PCM thickness should be higher. The numerical simulation has also been conducted considering actual weather conditions into account for three consecutive days with four different PCM (RT-26, RT-25, n-octadecane and RT-28). For three consecutive days, the percentage reduction of heat transport to the indoor environment is obtained 33.18%, 33.94%, 34.40% and 37.13% by using RT-26, RT-25, n-octadecane and RT-28 PCM, respectively.

Introduction

According to the international energy agency, the building sector is responsible for 24% of the world's total CO_2 emission and 40% of the world's total primary energy consumption [1]. To reduce CO_2 emission, we need renewable energy sources that can supply energy for various applications in the buildings. The solar energy is the most suitable renewable energy source for building energy supply. However, it is intermittent that creates a mismatch in energy supply and demand, therefore we need some energy storage devices that can store surplus energy of day time and shifts it night time. The phase change materials (PCM) can be utilized for this purpose [2–7]. Several researchers have investigated the utility of PCM and nano-PCMs in building applications [8–12]. These studies indicate that PCM can be applied to walls, glass, floor, and roofs which reduces the cooling cost of building significantly in comparison to active cooling cost [13–15]. The use of phase change material board (PCMBs) at the building wall can save electricity up to 13.10% however it does not offer considerable economic benefits [16]. The presence of a PCM in building envelope gives rise to an abrupt modification of the energies entering and exiting through the internal and external surface of wall [5,17]. The application of PCM with geo-cooling can save electricity consumption in buildings around 24–40% [18]. An experimental study showed that the application of PCM causes a daily average peak heat flux reduction for individual walls up to 25.4% however hourly average peak heat flux reduction for the sum of all four walls up to 20.1% [19]. Souayfane et al, [20] conducted the economic analysis of a transparent insulation material and phase change materials (TIM-PCM wall) wall under different climates. The results indicated that in polar and subarctic climates, the application of the TIM-PCM wall could be of high economic value and hence the investment may be attractive, with payback period in the range of 8–10 years approximately. Mehdaoui et al. [21] conducted numerical simulation and thermal testing of test cells on a small scale and subjected to the thermal stresses. They found that during the heating phase, the temperature inside the PCM shelter appears constant about 28 °C but it varied between 29 and 40 °C inside the test room without the PCM wall. These studies indicate that the application of PCM in building walls reduces the heat transfer rate in the building wall that reduces the temperature fluctuation in the buildings.

In the above-mentioned literature, the assessment of building walls utilizing PCM mostly uses heat flux and temperature variations at the indoor surfaces, the peak temperature of indoor and outdoor temperature. However, it is of practical importance to consider the effect of various parameters such as the PCM layer at a different position in the wall, PCM layer thickness and effect of melting temperature of PCM. To understand the cooling load reduction, it is also reasonable to see the temperature characteristics of different layers in the PCM integrated building wall. The present study has been conducted to address all the above-mentioned concerns regarding PCM integrated building wall. The

* Corresponding author.
E-mail addresses: k1091kant@gmail.com (K. Kant), ashukla@rgipt.ac.in (A. Shukla), asharma@rgipt.ac.in (A. Sharma).

https://doi.org/10.1016/j.egycc.2020.100008
Received 17 December 2019; Received in revised form 4 July 2020; Accepted 22 July 2020
Available online 21 August 2020

Nomenclature

C_p	specific heat [J/kgK]
F	view factor
g	acceleration due to gravity [m/s^2]
H	height of wall [m]
L_f	latent of fusion [J/kg]
n	normal vector on the boundary
q	heat flux [W/m^2]
T	temperature [K]
T_m	melting temperature [K]
ΔT	half of transition temperature [K]
t	time [s]
u	velocity in x-direction [m/s]
v	velocity in y-direction [m/s]
x	coordinates in x-direction [m]
y	coordinates in y-direction [m]

Greek symbols

ρ	density [kg/m^3]
λ	thermal conductivity [W/mK]
α	absorptivity
ε	emissivity
μ	dynamic viscosity [Pa•s]
γ	thermal expansion coefficient of air
β	thermal expansion coefficient of PCM

Subscript

a	air
w	wind
l	liquid
s	solid
amb	ambient
in	indoor

Acronyms

FB	fiberglass
gyp	gypsum
ext	external temperature
PCM	phase change material
OSB	oriented strand board

thermal model of a typical building wall incorporating PCM is developed considering heat and mass transfer in the melted PCM. The numerical simulation has been conducted considering constant heat flux at the outer surface of the wall as well as the actual weather condition of the City Rae Bareli (Latitude and longitude coordinates are: 26.23 N, 81.24 E), India with four different PCM. The melt fraction of and heat flux at the inner surface of the wall has been calculated for each case and discussed.

In the first part of the paper, we present a description of the numerical model of a typical building wall incorporating PCM and its thermophysical properties. In the next part of the paper we present: (i) the mathematical formulations considering convective heat transfer in the PCM for the simulation work; (ii) a short description on the boundary conditions that have been used for numerical simulations; (iii) the grid size, computational procedure, and model validation. Successively, the results of the present study have been presented for constant heat flux as well as the actual weather conditions of the city Rae Bareli. Finally, the outcomes of the present study have been presented in the conclusions section.

Model description

Fig. 1 depicts a typical wall structure used for the present study. The wall without incorporating PCM has been called the control wall in the

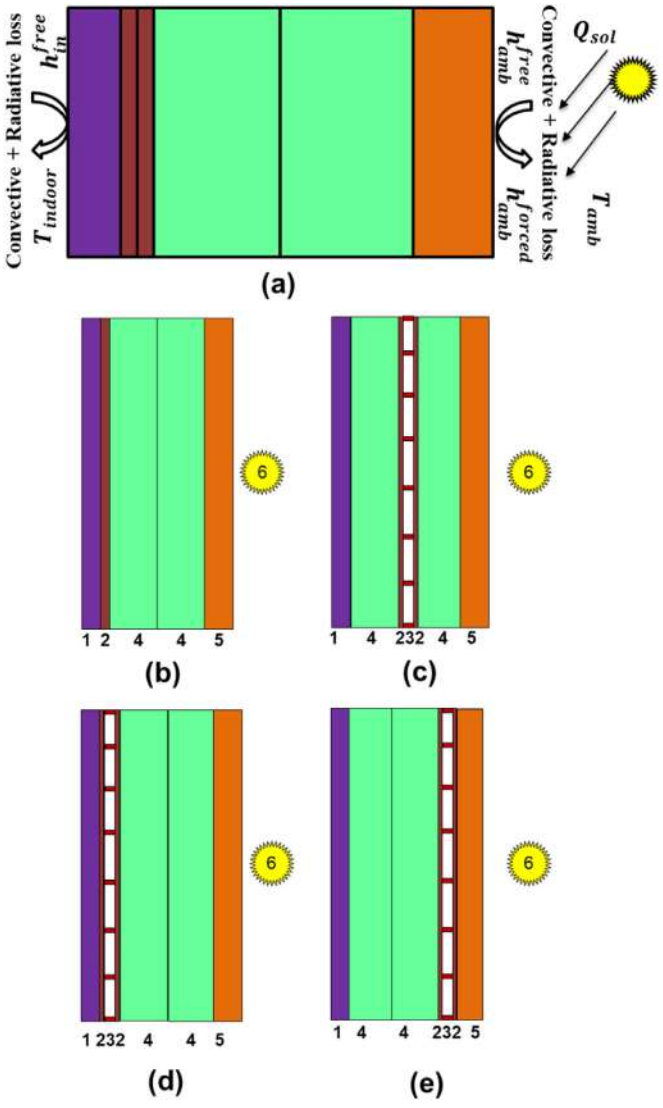

Fig. 1. Construction of wall (a) main heat transfer path to and from the wall (b) control wall, (c) PCM is placed in between the fiberglass; (d) PCM is placed at next to gypsum layer, (e) PCM is placed next to the fiberglass.
1: Gypsum, 2: polyacrylic plastic, 3: PCM, 4: Fiberglass, 5: OSB (oriented strand board), 6: The heat source.

present study. The configuration of the control wall is the same as a typical North American residential wall [22]. The wall with the height 1 m consists of gypsum wallboard (12.7 mm) attached with Acrylic plastic container (2.0 mm each, to cancel the effects of the container used for PCM storage), the Fiberglass insulation layers (44.5 mm for each layer) and an Oriented Strand Board (OSB) (20.5 mm). OSB is an engineered, waterproof, and heat-cured board made up of layering rectangular-shaped strands of wood arranged in cross-oriented patterns with acceptable structural and thermal properties. OSB is widely used in the United States for wall sheathing, floor underlayment, roof cover, and I-joists in commercial and residential buildings [23]. The PCM is filled in the 2 mm thick Acrylic plastic cavity of height 97.8 mm. The dimension of the container is shown in Fig. 2. The solar radiation incident on the OSB and some part of incident solar radiation absorbed by the OSB and remaining are thrown back without absorbing the atmosphere. The absorbed solar radiation starts increasing the temperature of the wall. The heat reflected back to the environment and indoor environment by the conduction, convection and radiation as depicted in Fig. 1. A part of the absorbed energy by wall is stored in PCM which is

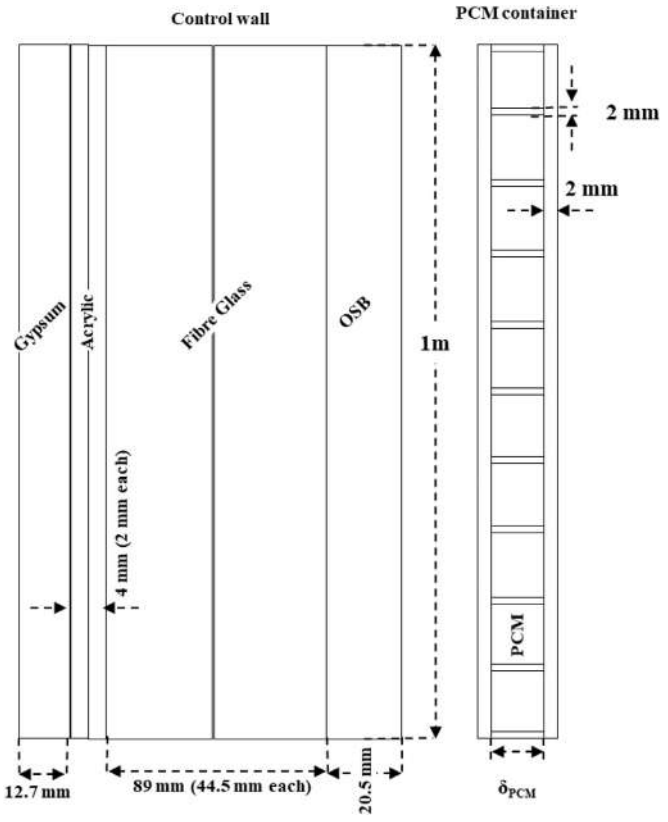

Fig. 2. The dimensions of the control wall and PCM Container.

filled inside the building wall during the sunshine hours (when energy supply is high) and released during off sunshine hours (when the energy demand is high). By this way, the surplus energy of sunshine hours shifted to the off-sunshine hours. The thermo-physical property for the different layers of a typical building wall is given in Table 1.

In the present study, the indoor air temperature is kept constant on 23 °C with natural convection and radiative heat loss to the indoor environment. At the outer surface of the wall, a constant heat flux of 750 [W/m^2] applied at the OSB layer surface which mimics incident solar radiation. The forced convective and radiative heat loss is considered at the outer surface of the wall. The outer ambient temperature has been considered 25 [°C]. The study has also been conducted for actual weather conditions to see the heat transfer characteristics of a typical North American wall.

Mathematical formulations for the simulation work

To study the heat transfer characteristics of a typical building wall with PCM at a different position, the conceptual design of the typical building is shown in Fig. 1. Several assumptions have been made for the mathematical modeling of building the wall. The assumptions are as follows [27–29]:

- The properties of different layers of the wall are isotropic and homogenous.
- The solar radiation incident of the wall is equally distributed everywhere.
- The melted PCM inside the container is Newtonian and incompressible.
- Three-dimensional convection and radiation inside the PCM are neglected.
- Convection mode of heat transfer is also considered inside the PCM.

The heat transfer study has been conducted considering each layer of the wall. The different layers of the building wall with its dimensions are

Table 1
Thermophysical properties of PCM and building wall materials.

Material/ property	Density [kg/m^3]	Specific heat [J/kgK]	Thermal conductivity [W/mK]	Melting temperature [°C]	Latent heat [kJ/kg]	Kinematic viscosity [m^2/s]	Thermal expansion coefficient [1/K]
PCM (n-octadecane) [24]	814(s), 775(l)	1934(s), 2196(l)	0.35(s), 0.149(l)	28.2	245	5.00×10^{-6}	9.10×10^{-4}
RT-28 [25]	880(s), 750(l)	2000 (both phase)	0.2 (both phase)	28.0	250	26.32×10^{-6}	1.25×10^{-3}
RT-26 [26]	880(s), 750(l)	2000 (both phases)	0.2 (both phase)	26.0	180	26.32×10^{-6}	1.25×10^{-3}
RT-25 [27]	785(s), 749(l)	1800(s), 2400(l)	0.19(s), 0.18(l)	25.0	232	1.79×10^{-6}	1.00×10^{-3}
Gypsum [23]	574	1100	0.60	*	*	*	*
Fibre Glass[23]	150	700	0.04	*	*	*	*
OSB [23]	800	1450	0.13	*	*	*	*
Acrylic Plastic	1470	1190	0.18	*	*	*	*

* Not applicable, (s) stands for solid, (l) stands for liquid.

depicted in the schematic diagram shown in Fig. 2. Over the inner and outer surface of the wall, the convective and radiative heat loss has been considered. Inside the layers of the control wall, only the conductive mode of heat transfer is considered. Inside the PCM layer of the wall, the conductive and convective both mode of heat transfer is considered. The mathematical formulation used for present simulation work is given in the following subsection :

Heat transfer model

Heat transfer model over building wall inner and outer surface

The main heat transfer path to and from the building wall and environment is convection and radiation. Heat loss occurs from building wall to the indoor environment due to the longwave radiation and natural convection. The convective heat transfer at the inner surface of the wall is only due to natural convection, which is also known as free cooling [7]. At the inner surface of the wall:

$$-\lambda_{gyp}\frac{\partial T}{\partial x} = h_{in}^{free}\left(T_{in} - T_{gyp}\right) + \varepsilon_{gyp}F\sigma\left(T_{in}^4 - T_{gyp}^4\right) \tag{1}$$

where h_{in}^{free} is the natural convection heat transfer coefficient at the Gypsum layer inner side and its value is taken from Kant et al. [8], σ is Stefan–Boltzmann and its value is approximately 5.67×10^{-8} (W/(m^2 K^4)), T_{in} is indoor air temperature, T_{gyp} is outer Gypsum layer temperature, ε_{gyp} is gypsum layer emissivity and its value is 0.85 [30], F is the view factor and in the present study, its value is considered unity. At the outer surface of the building wall, the convection heat transfer with the long and shortwave radiation is considered. As the building wall is vertical, therefore the ambient temperature is considered as the sky temperature and view factor (F) is 1 to calculate heat loss to the ambient in the form of longwave radiation. The convection heat transfer occurs due to the free cooling of OSB as well as convective heat transfer due to wind velocity. At the outer surface of the building wall:

$$\begin{aligned}-\lambda_{OSB}\frac{\partial T}{\partial x} &= \left(h_{amb}^{free} + h_{amb}^{forced}\right)\left(T_{amb} - T_{OSB}\right)\\ &\quad+\varepsilon_{OSB}F\sigma\left(T_{amb}^4 - T_{OSB}^4\right) + \alpha_{OSB}Q_{sol}(t)\end{aligned} \tag{2}$$

where h^{free} and h^{forced} are natural and forced convective heat transfer coefficient at the OSB layer outer side and its value is taken from Kant et al. [8]. T_{amb} and T_{OSB} are ambient and OSB layer temperatures, respectively. The emissivity of the OSB layer (ε_{OSB}) is taken 0.93 [31] and. The α_{OSB} is absorptivity of the OSB layer and it's is value is 0.9 [31] and Q_{sol} is heat flux which mimics incident solar radiation.

Heat conduction model inside the wall layers

Inside the solid part of the control wall i.e. Gypsum layer, Acrylic plastic, Fiberglass and OSB the pure conductive mode of heat transfer is considered. The heat transfer equation applied over the wall and it is given by [32]:

$$\rho C_p\frac{\partial T}{\partial t} + \nabla(-\lambda\nabla T) = 0 \tag{3}$$

where ρ, C_p, and λ are the density, specific heat and thermal conductivity of layer respectively.

Heat conduction and latent heat storage model inside the PCM layer

The heat transfer diffusion equation applied inside the PCM layer which can be given by [28]:

$$\rho_{PCM}C_{p,PCM}\frac{\partial T}{\partial t} + \nabla\left(-\lambda_{PCM}\nabla T\right) + \rho_{PCM}C_{p,PCM}\vec{u}\nabla T = 0 \tag{4}$$

where ρ_{PCM}, Cp_{PCM} and λ_{PCM} are the temperature dependent density, specific heat and thermal conductivity of PCM respectively. The velocity field $\vec{u}$ in Eq. (4) is quantified by the Navier–Stokes equation in the incompressible fluid. The temperature dependent density of the PCM can be modeled using Eq (5).

$$\rho_{PCM}(T) = \rho_{s,PCM} + \left(\rho_{l,PCM} - \rho_{s,PCM}\right)\theta(T) \tag{5}$$

where $\rho_{s,PCM}$ and $\rho_{l,PCM}$ is the solid and liquid PCM density and the value of function $\theta(T)$ grows linearly in the transition zone as:

$$\theta(T) = \begin{cases} 1 & T > \left(T_m + \Delta T\right) \\ \frac{T - T_m + \Delta T}{2\Delta T} & \left(T_m - \Delta T\right) \le T \le \left(T_m + \Delta T\right) \\ 0 & T < \left(T_m - \Delta T\right) \end{cases} \tag{6}$$

where T_m is the mean of melting temperature and ΔT the half range of transition temperatures and its value is 1 °C. The value of function $\theta(T)$ is 0 in the solid-state and 1 in the melted state. The temperature dependent heat capacity of PCM can be given as:

$$C_{p,PCM}(T) = C_{ps,PCM} + \left(C_{pl,PCM} - C_{ps,PCM}\right)\theta(T) + L_f D(T) \tag{7}$$

where $C_{ps,PCM}$ and $C_{pl,PCM}$ is the specific heat capacity in the solid and liquid state of PCM, respectively. L_f is the latent heat of the fusion and $D(T)$ is the delta function and its value is given by [27]:

$$D(T) = e^{\left(\frac{-T(T-T_m)^2}{\Delta T^2}/\sqrt{\pi\Delta T^2}\right)} \tag{8}$$

The value of function $D(T)$ is zero everywhere except in the temperature range of T_m-ΔT to T_m+ ΔT. The main reason for the use of delta function is to distribute the latent heat equally to both sides of the melting temperature in the range of transition temperature. The integral value of the function $D(T)$ is 1. The thermal conductivity of PCM also depends on the temperature and it can be given by:

$$\lambda_{PCM}(T) = \rho_{s,PCM} + \left(\lambda_{l,PCM} - \lambda_{s,PCM}\right)\theta(T) \tag{9}$$

where λs_{PCM} and λl_{PCM} is the thermal conductivity in the solid and liquid state of PCM respectively.

Momentum transfer in the PCM layer

It is supposed that the melt PCM is Newtonian and incompressible. The momentum transfer equation modified as follows to model the phase transition process for the PCM:

$$\begin{aligned}&\rho_{PCM}\frac{\partial\vec{u}}{\partial t} + \rho_{PCM}\left(\vec{u}\cdot\nabla\right)\vec{u} - \mu_{PCM}\nabla^2\vec{u}\\ &= -\nabla P - \omega(T)\vec{u} - \rho_{l,PCM}\left(1 - \beta\left(T - T_m\right)\right)\vec{g}\end{aligned} \tag{10}$$

where μ_{PCM} is the dynamic viscosity of melted PCM, the last term in the right-hand side of Eq. (10) is buoyancy force given by the Boussinesq approximation. The second term in the right-hand side of the momentum equation is inspired by the Carman–Koseny relation in a porous medium and the value of the with the function $\omega(T)$ is given by Eq. (11) and the function ∇P from Darcy's law, as presented by Voller and Prakash [33] and Brent et al. [34]. If we assume that, the flow is laminar the value of ∇P is given by Eq. (12):

$$\omega(\mathrm{T}) = \frac{\varphi(1-\theta(T))^2}{\left(\theta^2(T) + \tau\right)} \tag{11}$$

$$\nabla P = \frac{-\varphi(1-\theta(T))^2}{\theta^3(T)}\vec{u} \tag{12}$$

where φ and τ are the constant and depends on the morphological structure of PCM. The value of φ is chosen 10^6 kg/m^{3}s [35] and this value is chosen as in the numerical benchmark [36]. Increasing the value of coefficient φ leads to a reduction in the flow of liquid PCM in the transition zone. The value of constant τ is selected very low therefore the Eq. (11) become effective, however, $\theta(T)$ is zero. The substantial value of τ is fixed at 10^3. In the increase in the temperature of PCM the value of θ becomes 1 which results in the value of the function $\omega(T)$ becomes zero.

Boundary conditions

The indoor air temperature (T_{in}) in the present study is set to 23 °C for human comfort [37]. At the PCM container wall, the no-slip condition is applied therefor the velocity of melted PCM at the container wall is zero. At the top and bottom of the control wall symmetry boundary is considered i.e. $-n.q = 0$ and $K-(K.n)n = 0$, where $K = (\mu \cdot \nabla^2 \vec{u}) \cdot n$, q is the heat flux and n is the vector normal to the surface.

Grid, computation and model validation

The partial differential equation subjected to initial and boundary conditions solve concurrently using the commercial package of COMSOL 5.3a which is based on the finite element method. The higher grid size is considered in the solid layers of the building wall in comparison with the PCM layer as the mesh size of wall layers does not much affect numerical results as compared to the PCM layer. The grid size is reduced at the boundary of the PCM layer, which reduces the error in the calculation as there is interaction in the solid layer to the melted PCM. As the numerical results of the calculation depend on the grid size of each layer there for the study has been conducted for various mesh sizes (i.e. 15,195, 23,354 and 107,774 number of element) From the study, it was found that with the reduction in mesh size (i.e. increment in the number of mesh element), will not much affect the calculated results. Therefore for the sake of accuracy, the maximum 107,774 number of elements have been taken for the present study. For the present study, the grid size is selected such that the numerical results of the model are independent of grid size. The transient heat transfer study has been conducted using the heat transfer and fluid flow module of COMSOL Multiphysics 5.3a software.

To apply our developed thermal model for further calculation, we have first validated it with the experimental studies. The developed thermal model with the PCM has also been validated with the application of PCM performed by Biwole et al. [27]. For the model validation the 2 [cm] thick PCM layer considered in between two 4 [mm] thick aluminum layer of height 13.20 [cm]. The heat transfer coefficient at the front and back surface of the aluminum layer is 10 [W/m^2 K] and 5 [W/m^{2}K]. The external temperature to both sides of the aluminum plate is considered 20 [°C] and heat flux 1000 [W/m^2], which mimics the incident solar radiation. The calculation from the present simulation model, in terms of temperature, are compared with the calculations done by Biwole et al. [27] and shown in Fig. 3 This comparative study clearly shows that the developed thermal model is in good agreement with the results of an experimental and numerical study carried out by Biwole et al. [27]. Such a comparative study puts a stringent test of the consistency of our model and its predictions before using it further.

Result and discussion

To understand the heat transfer characteristics of the wall, the study has been conducted for the constant heat flux subjected at the outer surface of the OSB layer and with the actual weather condition of City Rae Bareli. The results and discussion of the present study have been presented in the six subsections. In the first subsection, the temperature and velocity field in the melted PCM has been discussed when the PCM layer is placed in between two fiberglass layers and the outer surface of the OSB layer is subjected to constant heat flux. In the second subsection, the effect of the PCM layer positing has been discussed. In the second, third, fourth and fifth subsection the effect of the PCM layer position, PCM layer thickness and the melting temperature has been discussed correspondingly. In the last subsection, the discussion has been made on the results obtained with the actual weather condition.

Temperature and velocity field

To see the heat transfer characteristics of building wall containing phase change materials the study has been conducted with the constant heat flux of 750 [W/m^2], which mimic solar radiation incident on the OSB layer. The ambient and indoor air temperatures have been considered 23 °C and 25 °C, respectively. The initial temperature of the wall has been considered equal to the indoor air temperature and wind speed at the front surface of the OSB layer is 2 [m/s] has been considered in the present study. The n-octadecane has been considered as PCM for the thermal energy storage in the building wall. The solar radiation incident on the OSB layer outer surface and raises building wall temperature. After a certain time, the building wall temperature reaches to melting temperature of PCM that is filled in the cavity of the wall and starts melting. During the phase transition of PCM, the temperature of the building wall maintained at the melting temperature of PCM. Fig. 4 represents the temperature characteristics of the wall at 7 different time span. The study is conducted when the PCM layer is placed in between two fiberglass layers. In Fig. 4 the x-axis represents the distance from the gypsum layer to the OSB wall outer surface and the y-axis represents temperature variation in the wall layers. Initially, the temperature of the inner surface of the gypsum layer was 23.00 °C and reaches 24.30 °C after 720 min. The maximum temperature of the outer surface of the OSB layer reaches 67.20 °C after 720 [min]. The surface temperatures of Gypsum layer at 100 [min], 300 [min], 450 [min], 500 [min], 550 [min],

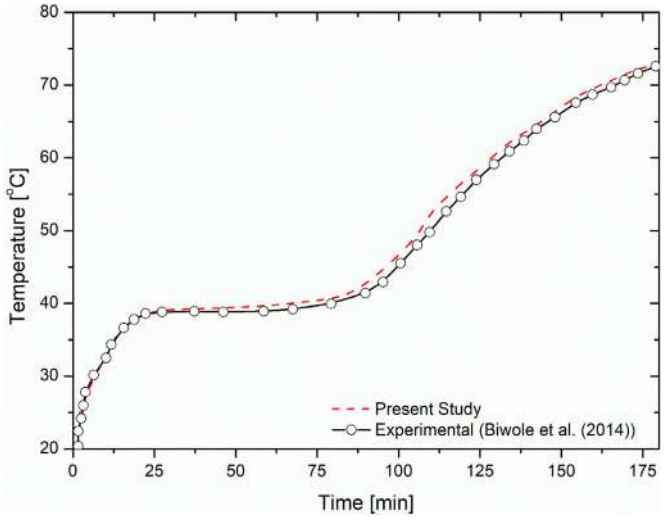

Fig. 3. Model validation with Biwole et al. 2014 [27].

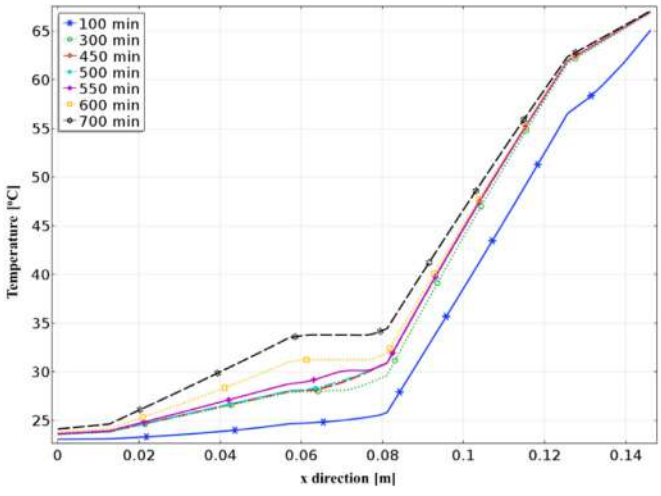

Fig. 4. Temperature variation of building wall containing PCM in between two fiberglass layers.

600 [min], 700 [min] are 23.08 [°C], 23.59 [°C], 23.61 [°C], 23.62 [°C], 23.70 [°C], 23.90 [°C], 24.24 [°C], respectively, and surface temperatures of OSB layer at same time are 65.10 [°C], 66.92 [°C], 67.00 [°C], 67.00 [°C], 67.01 [°C], 67.02 [°C], 67.12 [°C], respectively. The temperature of each layer in the wall decreases linearly from the OSB layer to the gypsum layer except the PCM layer. The temperature of the gypsum surface remains constant at 23.6±0.1 °C during the melting of PCM from 200 [min] to 550 [min], which can be seen by Fig. 4. The temperature profile of the wall depending on the thermophysical properties of construction material, convective and radiative heat transfer from the wall to the surroundings and radiation incident on the building wall surface. In the present study, we have used fiberglass as an insulating material in the wall which prevents the heat transport from the wall to the indoor environment and increases the temperature [9,22,38–40].

The variation of heat flux at the inner surface of the Gypsum layer and solid fraction of PCM with time is shown in Fig. 5. Solid fraction (SF) is a dimensionless number, and its value is given by the following relation:

$$SF = \left(1 - \frac{Volume\ of\ melted\ PCM}{Total\ volume\ of\ PCM}\right) = \left(1 - \frac{Energy\ stored\ in\ the\ form\ of\ latent\ heat\ (\Delta E)}{Latent\ heat\ of\ fusion(L_f)}\right) = \left(\frac{Energy\ that\ can\ be\ stored\ in\ the\ form\ of\ latent\ heat}{Latent\ heat\ of\ fusion(L_f)}\right) \quad (13)$$

The SF is the percentage of PCM that remains in solid-state after a certain time. Initially, the indoor temperature and the initial temperature of the wall are similar therefore the there is no heat transfer from the wall to the indoor environment. As time increases the heat transfer from the wall to the indoor environment starts increasing and it becomes constant when PCM starts melting which can be seen by Fig. 5. The PCM starts melting at 170 [min] and up to this time, the heat flux at the gypsum layer surface increasing sharply from 0 [W/m^2] to 2.10 [W/m^2]. From the 100 [min] to the 250 [min] the heat flux increases sharply from 0.44 [W/m^2] to 3.50 [W/m^2] and 22.5 % PCM completely melted. From 250 [min] to 550 [min] the value of heat flux increases gradually and reaches 4.37 [W/m^2] from 3.50 [W/m^2] with an increment of 0.87 [W/m^2], and the same time PCM is completely melted. During the melting phase, PCM absorbed excess heat of the building wall, therefore the value heat flux at the gypsum layer surface does not increase sharply. After the 550 [min], the heat flux starts increasing sharply as the PCM is completely melted and its value becomes 8.46 [W/m^2] at 720 [min]. Fig. 5 shows the variation of heat flux at the gypsum layer also when

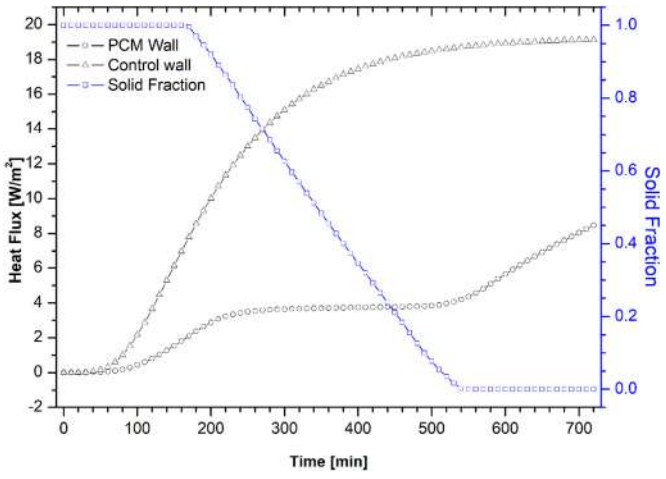

Fig. 5. Average heat flux variation with time at the gypsum layer inner surface and solid fraction of PCM: (Solid fraction (SF), Heat flux).

there is no PCM layer in the wall (control wall case). The heat transport to the indoor environment is higher with the control wall as compared to wall incorporated with PCM. With the control wall, heat flux at the gypsum inner surface reaches 19.14 [W/m^2] at 720 [min] and the total 72.93% heat transfer reductions obtained when the PCM layer was placed in between two fiberglass layers.

Fig. 6 represents the velocity field in the PCM cavity at different time instances by the color contour of the arrow. The minimum and maximum velocity field in the PCM container are 0 [m/min] and 9.87×10^{-6} [m/min]. As the constant heat flux is applied at the OSB outer surface, therefore the heat is transported to the PCM from the OSB layer by the conduction. The PCM absorbs heat and starts melting, the melted PCM have lower density as compared to solid PCM, therefore, melted PCM move upwards direction. The PCM which has a comparatively lower temperature moves downward direction, therefore the velocity field has been generated in the melted PCM, which increases the convective heat transfer in the PCM domain. The velocity field near the right acrylic layer is higher due to the higher temperature gradient near the wall and has positive (+ve) *y*-direction as shown in Fig. 6 by the color contour. The velocity field near solid PCM has a negative (-ve) *y*-direction downward direction. The average velocity of melted in the container at 400 [min], 450 [min], 500 [min], 550 [min] and 600 [min] is 1.64×10^{-7} [m/min], 7.77×10^{-7} [m/min], 1.65×10^{-6} [m/min], 2.58×10^{-6} [m/min] and 2.87×10^{-6} [m/min] respectively. Due to the density difference in solid and liquid PCM the melted PCM collected in the upper part of the container which leads to higher melted PCM in the upper part of the cavity as compared to the lower part.

During the melting of PCM, there are two components of the velocity field induced in the cavity i.e. *x* and *y*-component. Fig. 7 represents the *y*-component velocity field in the middle of the cavity at a different time. In the figure, the *x*-axis represents the distance from the surface of the gypsum layer and the *y*-axis represents y component of the velocity field. The value of the *y*-component of the velocity field (*v*) near the right side of the container starts increasing in the positive as well as negative direction with time. When the melted PCM touches the left side of the container the value of the *y*-component of the velocity field starts decreasing in the positive and negative direction with time and it further starts increasing in the positive and negative direction when the PCM is completely melted.

Effect of PCM layer position

To see the effect of PCM layer position the study has been conducted for four different cases: (i) when there is no PCM (control wall) (ii) when PCM layer is placed in between the gypsum layer and fiberglass layer (GYP-PCM-FG), (iii) when PCM layer is placed in between fiberglass and OSB layer (FG-PCM-OSB) and (iv) when the PCM layer is placed in between the two fiberglass layers (FG-PCM-FG). The initial and boundary conditions are the same as in the previous section 4.1. Fig. 8 represents the heat flux variation on the indoor gypsum layer surface and solid fraction of PCM with time when PCM layer is placed at different positions in the building wall. The maximum heat is transported to the indoor environment when there is no PCM layer in the wall and heat flux is reached 19.14 [W/m^2] at 720 [min]. The total energy transported to the indoor environment without PCM in the wall is 579.29 [kJ] in 720 [min]. When the PCM layer is placed in between the gypsum layer and fiberglass, the maximum heat flux value at the gypsum layer surface reaches at 17.74 [W/m^2] and total energy transported to the indoor environment is 480.74 [kJ] in the same duration which is 17.01% lower as compared to the control wall. In this case, PCM does not completely melt because of enough heat is not reach to the PCM layer due to fiberglass insulation therefore PCM layer temperature does not reach above to its melting temperature and heat transfer in the PCM layer is purely conductive. The thermal resistance of the gypsum layer is not enough to block the heat transport to the indoor environment. When the PCM layer is placed in between the fiberglass and OSB the heat transfer rate from

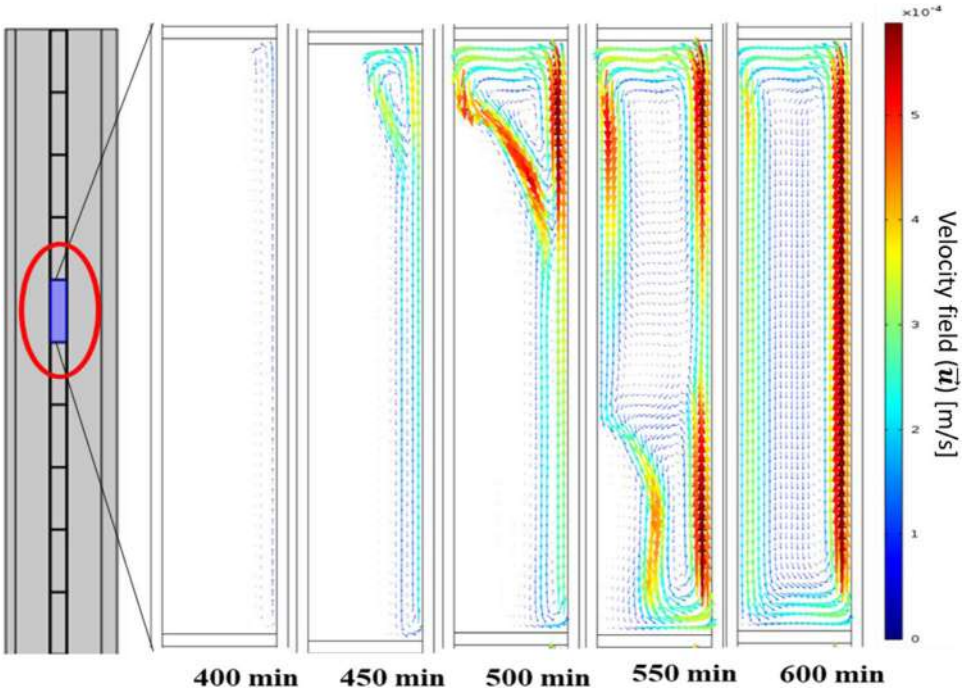

Fig. 6. Velocity field in the PCM container at a different time.

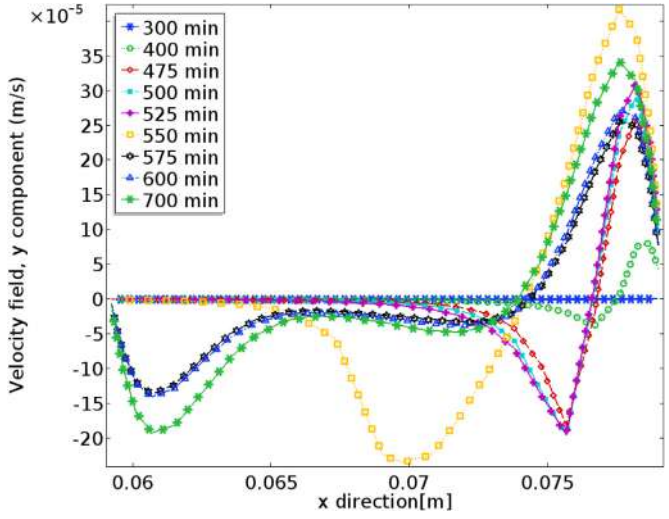

Fig. 7. Variation of the y-component of the velocity field at the mid-height of the cavity.

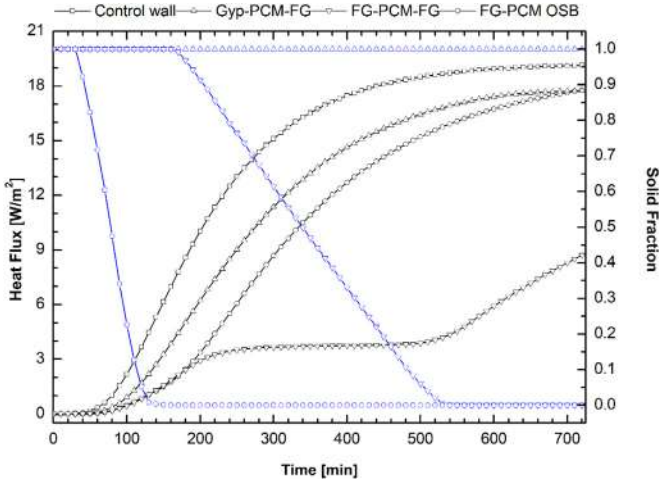

Fig. 8. Effect of PCM layer position on average heat flux variation at the gypsum layer inner surface and solid fraction of The PCM: (Solid fraction (SF), Heat flux).

OSB to PCM is higher, therefore, the PCM layer melt in the shorter time duration and maximum heat flux is reached 17.82 at 720 [min] which is like the previous case when the PCM layer is placed in between the gypsum layer and fiberglass layer, however, the energy transported to the indoor environment is lower. In this case, PCM starts melting from 30 [min] and completely melted at 140 [min] the total time duration of complete melting is 110 [min] and total energy transported to the indoor environment is 433.08 [kJ] which is 25.24% lower as compared to control wall. When the PCM layer is placed in between two fiberglass layers the maximum heat flux reached at the value of 8.71 [W/m^2] at 720 [min]. In this case, the PCM starts melting at 165 [min] and completely melted at 545 [min]. The total time duration for the complete melting of PCM is 380 [min] and the total energy transported to the indoor environment are 159.92 [kJ] which is 72.39 % lower as compared to control wall. The highest reduction of heat transported to the indoor environment is achieved for the case when the PCM layer is placed in between two fiberglass layers.

Effect of PCM layer thickness

The study has also been conducted for the four different thickness of PCM layer i.e. 1 [cm], 2 [cm], 3 [cm] and 4 [cm]. The variation of heat flux with time at the gypsum layer surface is shown in Fig. 9 for four different thicknesses of the PCM when the PCM layer is placed in between two fiberglass layers (FG-PCM-FG). The heat flux reduces with an increase in PCM layer thickness that results in the lower thermal energy transported to the indoor environment. The total energy transported to the indoor environment is 294.4 [kJ], 159.92 [kJ], 119.39 [kJ] and 107.27 [kJ] for 1 [cm], 2 [cm], 3 [cm] and 4 [cm] thick PCM layer respectively. The reduction in the energy transported to the indoor environment as compared to control wall is 49.17%, 72.39%, 79. 39% and 81.48% for 1 [cm], 2 [cm], 3 [cm] and 4 [cm] thick PCM layer respectively. For the 1 [cm] and 2 [cm] thick PCM layer the PCM has been completely melted in 290 [min] and 545 [min] respectively,

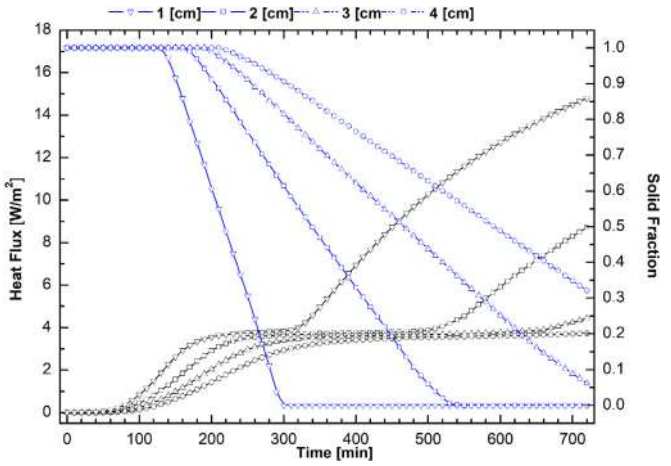

Fig. 9. Variation of average heat flux at the inner surface of the gypsum layer and solid fraction of PCM for different thickness of PCM layer: (Solid fraction (SF), Heat flux).

however 6.2 % and 32.14 % of PCM remain in solid phase for the 3 [cm] and 4 [cm] thick PCM layer respectively. The maximum heat flux value at gypsum layer surface is reached 14.79 [W/m^2], 8.71[W/m^2], 4.44 [W/m^2] and 3.73 [W/m^2] for 1 [cm], 2 [cm], 3 [cm] and 4 [cm] thick PCM layer respectively. For the lower thickness of the PCM layer, the heat flux becomes constant for shorter time duration and vice versa. For the all PCM thickness the heat flux at gypsum layer surface become constant value in the range of 3.5±0.5 [W/m^2] for time duration of 155 [min], 310 [min] and 420 [min] for the 1 [cm], 2 [cm], and 3 [cm] thick PCM layer, however for 4 [cm] thick PCM layer the total PCM has not been melted completely. The maximum heat flux at gypsum surface reaches 14.79 [W/m^2], 8.71 [W/m^2], 4.44 [W/m^2] and 3.73 [W/m^2] for 1 [cm], 2 [cm], 3 [cm] and 4 [cm] thick PCM layer respectively.

Effect of PCM melting temperature

The melting temperature of PCM is also affecting the heat transport rate to the indoor environment; therefore, the study has been conducted for the different melting temperatures to investigate the suitable phase change temperature of the PCM. Fig. 10 shows the variation of heat flux at gypsum layer surface and solid fraction of PCM at 24 [°C], 26 [°C], 28 [°C], 30 [°C], and 32 [°C] with time. For the lower melting temperature, the PCM starts melting earlier however for higher melting temperature

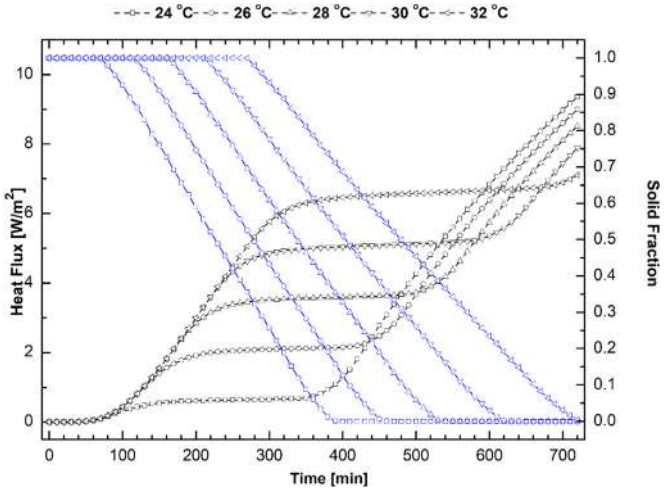

Fig. 10. Variation of average heat flux at the gypsum layer inner surface and solid fraction of PCM at different melting temperature with time (Solid fraction (SF), Heat flux).

the PCM starts melting later. The time duration for melting of PCM is 315 [min], 340 [min], 375 [min], 415 [min] and 450 [min] for 24 [°C], 26 [°C], 28 [°C], 30 [°C], and 32 [°C] melting temperature respectively. The total energy transported to the indoor environment is 123.95 [kJ], 138.34 [kJ], 154.97 [kJ], 176.20 [kJ], 204.48 [kJ] and percentage reduction in heat transported to the indoor environment is 78.60 %, 76.11 %, 73.24 %, 69.58%, 64.70 %, for 24 [°C], 26 [°C], 28 [°C], 30 [°C], and 32 [°C] melting temperature respectively. The maximum heat flux at gypsum surface reaches 9.35 [W/m^2], 8.99 [W/m^2], 8.52 [W/m^2], 7.89 [W/m^2] and 7.10 [W/m^2] for for 24 [°C], 26 [°C], 28 [°C], 30 [°C], and 32 [°C] melting temperature, respectively.

Fig. 11 represents the reduction of heat flux for different parameters i.e. PCM layer position in the wall, PCM melting temperature and

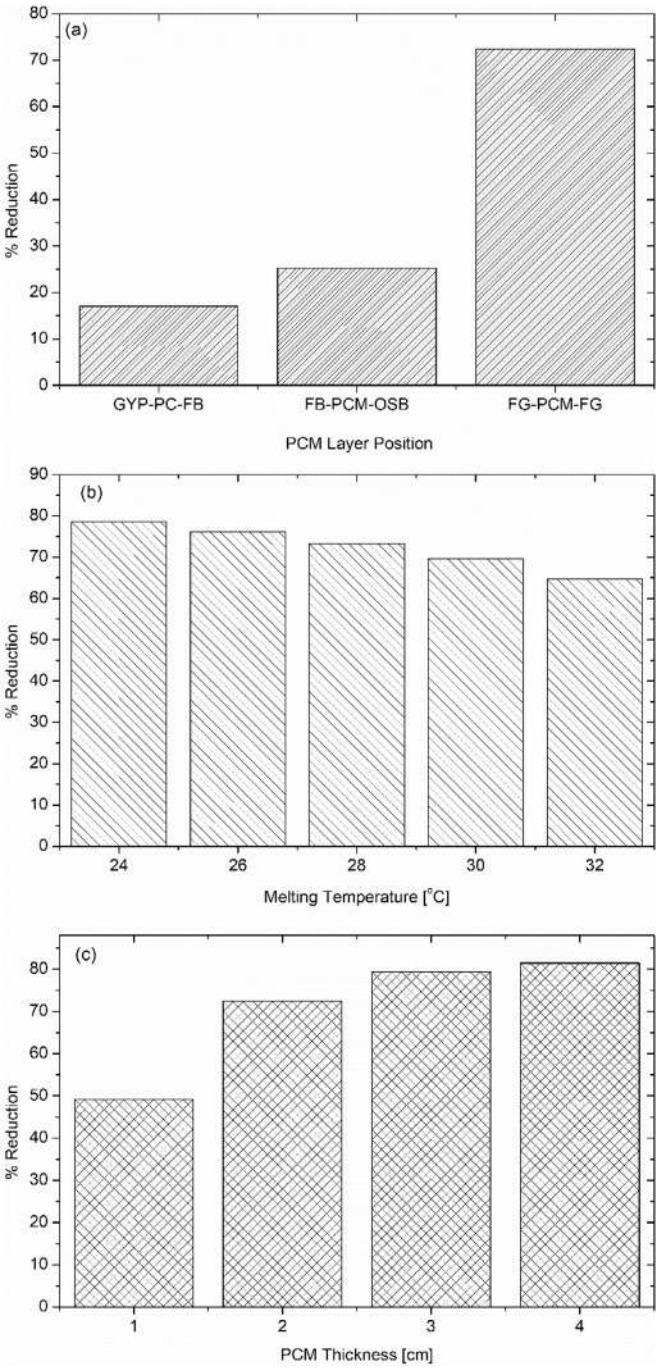

Fig. 11. Percentage (%) reduction in energy transported to the indoor environment for different parameter.

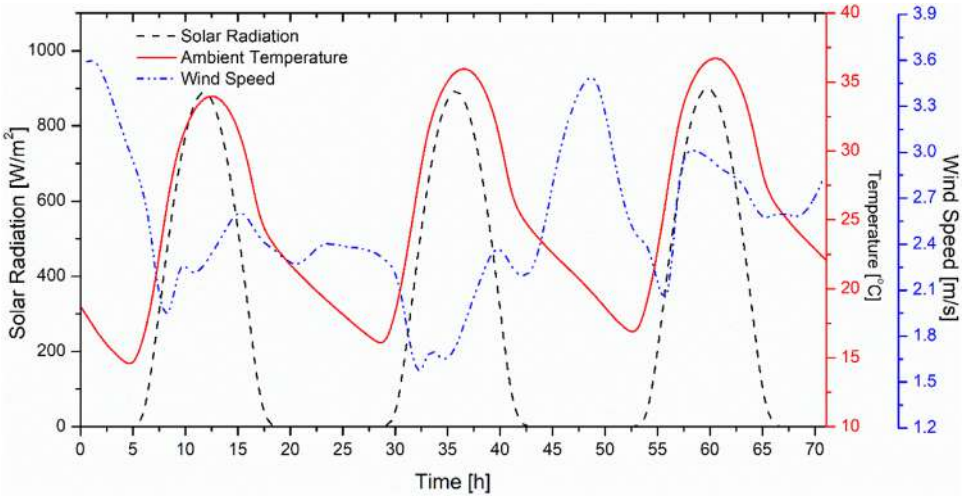

Fig. 12. Actual weather data for the city Rae Bareli, India used for numerical simulations [41].

PCM layer thickness. Fig. 11 (a) represents the % reduction of thermal energy transported to the indoor environment when the PCM layer is placed at a different location in the wall. Minimum 17.01% reduction is obtained when the PCM layer is placed in between the gypsum layer and the fiberglass layer. The maximum reduction is obtained when the PCM layer is placed in between the two fiberglass layers. In this case the melting temperature is 28.2 [°C] and PCM thickness is 2 [cm]. In Fig. 11 (b) the % reduction of thermal energy transported to the indoor environment at different melting temperature has been shown. The reduction in the thermal energy transported to the indoor environment has been decreasing with an increase in melting temperature. The higher reduction is achieved when the melting temperature is near to the indoor environment temperature. In this case, the PCM layer is placed in between the fiberglass layers, and PCM thickness is 2 [cm]. With the increase in PCM thickness the % reduction is increasing however after a certain thickness the % reduction becomes constant because the PCM layer has not been completely melting, which can be seen by Fig. 11 (c). In this case, the melting temperature is 28.2 [°C] and the PCM layer is placed in between two fiberglass layers.

Numerical simulation with actual weather conditions

The numerical simulation has been conducted considering the actual weather conditions of the city Rae Bareli. The weather data that has been taken for the present study is shown in Fig. 12. In this study, the indoor air temperature and initial temperature of the building wall are taken at 23 °C. The thickness of the PCM layer is 2 [cm]. The study has been conducted for the four different PCM which is commercially available in the market.

The numerical simulation started at midnight when there is no solar radiation and ambient temperature is lower than the wall temperature as shown in Fig 12. Due to lower ambient temperature, there is heat loss to ambient in the form of the convective and radiative heat transfer. In this way, wall temperature becomes similar to the ambient temperature. Solar radiation starts incidents on the building wall in the morning and when it is incident on the building wall, some parts of its absorbed by the wall and remaining reflected in surroundings. The absorbed solar radiation starts increasing the temperature of the building wall. When the building wall temperature becomes similar to the melting temperature of PCM filled in the cavity, PCM starts melting and absorbs heat isothermally. After the complete charging of PCM, it starts absorbing heat in the form of sensible heat and causes a temperature rise in the wall. As solar radiation increasing from morning to noon, therefore the temperature of building wall increasing in a similar fashion. However, during the melting of PCM, the temperature of the building wall becomes constant due to isothermal heat absorption PCM. Solar radiation starts decreasing from the afternoon and becomes zero in the evening, therefore the wall temperature also starts decreasing from noon to the evening due to the convective and radiative heat loss to the surroundings. When the solar radiation becomes zero in the evening, the heat loss from the wall still going on, and the temperature of the wall falling till the next morning when the solar radiation starts falling again on the wall. The cycle repeats every day by absorbing access heat in PCM incorporated in the building wall in the day time and releasee to surroundings in the night time. In this way, the cooling loads of the building are reduced.

Fig. 13 represents the variation of heat flux at the gypsum layer surface for four different PCM and control wall for three days when the PCM layer is placed in between two fiberglass layers. At the start of the simulation, the ambient temperature lower as compared to the initial value of wall temperature and there is no solar radiation falling on the OSB surface, therefore, the heat flux is in the negative direction. During this time the thermal energy transported from the indoor environment to the building wall. When the solar radiation starts falling on the OSB layer the temperature of the building wall starts increasing which leads to heat transport from the wall to the indoor environment. When the PCM starts melting, the heat flux at the gypsum layer becomes constant and it starts increasing further when the PCM is completely melted. For the first day of the numerical simulation, the maximum heat flux at the

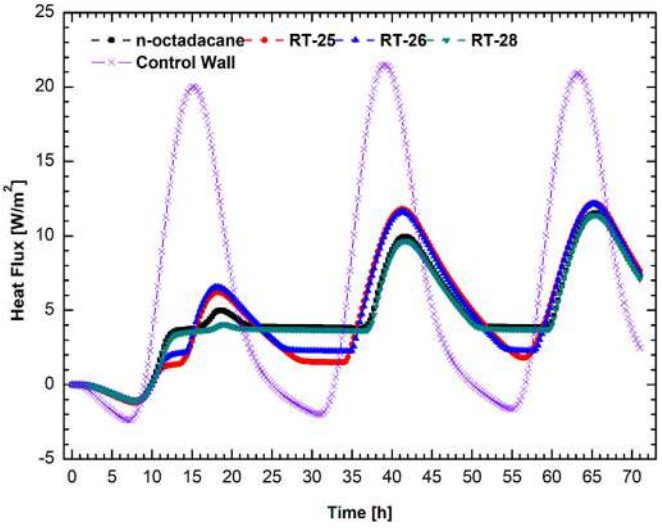

Fig. 13. Variation of heat flux on the gypsum layer with time considering actual weather condition with 2 [cm] thick PCM layer.

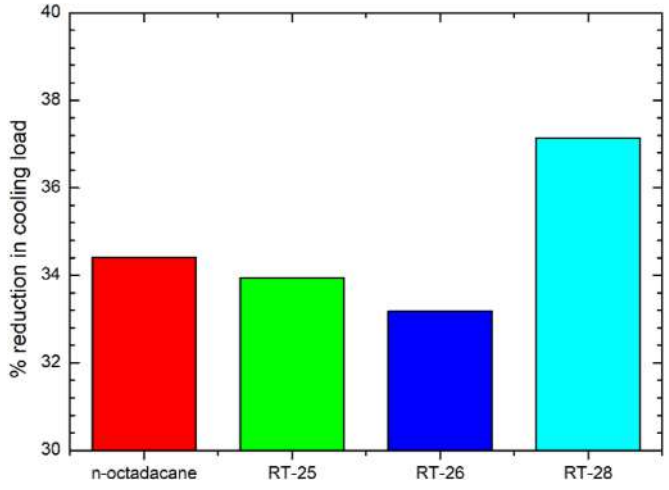

Fig. 14. Reduction in the cooling load with different PCM for three days.

gypsum layer is obtained with the RT-26 and minimum with the RT-28. For the second and third days of the numerical simulation, maximum heat flux is obtained with RT-25 and minimum with RT-28. Total 7.5%, 22.7%, 94.05%, 99.79% and 0%, 0.2%, 25.5%, 29.4% PCM has been solidifies after first day and second day simulation for the RT- 25, RT-26, RT-28 and n-octadecane respectively. The total energy transported through the building wall from outdoor to the indoor environment is 1253.40 [kJ], 1267.90 [kJ], 1192.80 [kJ] and 1244.60 [kJ] for RT-25, RT-26, RT-28, and n-octadecane respectively in three consecutive days. Fig. 14 shows the reduction of cooling load with four different PCMs for three consecutive days. The maximum reduction is reported by RT-28 PCM and minimum with the RT-26. The reduction in the cooling load has been reported 37.13% with the RT-28, 34.40% n-octadecane, 33.94% with RT-25 and 33.18% with RT-26. The importance of the present study lies in the utility of PCMs for the building sector. On one hand, the building sector utilizes one of the major chunks of energy globally, still, the solution varies due to different climatic conditions and availability of resources. Hence, such a study could be quite useful for bringing out commercial products in the application domains and would be very much complementary to the existing literature dealing with the application of PCMs in the building sector.

Conclusions

The main objective of the present study has been to develop a thermal model of a building wall incorporating phase change material and investigate the effect of the PCM layer position in the building wall, melting temperature of PCM and PCM layer thickness. The numerical simulation has been conducted for different parameters and concluded that:

(i) The highest heat transport reduction to the indoor environment is obtained when the PCM layer is placed in between two fiberglass layers and lowest when the PCM layer is placed in between the Gypsum layer and the fiberglass layer because of the fiber glass have lowest thermal conductivity and decreases the heat transfer to PCM, therefore, PCM melts in longer time duration which results in higher time lower heat transport to the indoor environment.

(ii) The heat transport to the indoor environment is reduced with an increase in the PCM layer thickness because of the higher PCM thickness, the higher amount of heat can be stored in the PCM layers which results in the lower heat transfer to the indoor environment.

(iii) The heat transport to the indoor environment minimum when the melting temperature of PCM closer to indoor environment temperature as there is a lower temperature gradient in between the wall and indoor air which results in lower heat transport.

The numerical simulation has also been conducted for three consecutive days with the actual weather condition of the Indian climatic conditions with four different PCMs. The percentage reduction of heat transport in three days to the indoor environment is obtained 33.18%, 33.94%, 34.40% and 37.13% for RT-26, RT-25, n-octadecane and RT-28 PCM respectively. The present developed thermal model can be used to predict the quantity and suitability of PCM in a building wall for given environmental conditions of any suitable location of installation. This could be used to construct more efficient and economical building walls incorporating PCM. Also, further research is required on developing the thermal model considering the orientation of the building wall and its experimental validation considering different locations. This also includes the possibility of exploring new low-cost PCMs to decrease the investment costs for buildings integrating such as walls and as a result, make them even more economically viable.

Declaration of Competing Interest

The authors declare that they have no known competing financial interests or personal relationships that could have appeared to influence the work reported in this paper.

Acknowledgment

The authors, A. Sharma and A. Shukla are thankful to the Council of Science and Technology, Govt. of U.P. India (Reference No. CST 3012-dt.26-12-2016) for providing research grants to carry out the research work at the RGIPT Jais, Amethi, India.

References

[1] IEA-International Energy AgencyEnergy Technology Perspectives 2017 – Catalysing Energy Technology Transformations, 1st ed., IEA, 2017 https://webstore.iea.org/energy-technology-perspectives-2017.
[2] A. Shukla, A. Sharma, M. Shukla, C.R. Chen, Development of thermal energy storage materials for biomedical applications, J. Med. Eng. Technol. 39 (2015) 363–368 https://doi.org/, doi:10.3109/03091902.2015.1054523.
[3] A. Sharma, V.V. Tyagi, C.R. Chen, D. Buddhi, Review on thermal energy storage with phase change materials and applications, Renew. Sustain. Energy Rev. 13 (2009) 318–345 https://doi.org/, doi:10.1016/j.rser.2007.10.005.
[4] D. Mazzeo, G. Oliveti, N. Arcuri, Definition of a new set of parameters for the dynamic thermal characterization of PCM layers in the presence of one or more liquid-solid interfaces, Energy Build. 141 (2017) 379–396 https://doi.org/, doi:10.1016/J.ENBUILD.2017.02.027.
[5] D. Mazzeo, G. Oliveti, N. Arcuri, A method for thermal dimensioning and for energy behavior evaluation of a building envelope PCM layer by using the characteristic days, Energies 10 (2017) https://doi.org/, doi:10.3390/en10050659.
[6] D. Mazzeo, G. Oliveti, Thermal field and heat storage in a cyclic phase change process caused by several moving melting and solidification interfaces in the layer, Int. J. Therm. Sci. (2018) https://doi.org/, doi:10.1016/j.ijthermalsci.2017.12.026.
[7] A. Arnault, F. Mathieu-Potvin, L. Gosselin, Internal surfaces including phase change materials for passive optimal shift of solar heat gain, Int. J. Therm. Sci. 49 (2010) 2148–2156 https://doi.org/, doi:10.1016/J.IJTHERMALSCI.2010.06.021.
[8] K. Kant, R. Pitchumani, A. Shukla, A. Sharma, Analysis and design of air ventilated building integrated photovoltaic (BIPV) system incorporating phase change materials, Energy Convers. Manag. 196 (2019) 149–164 https://doi.org/, doi:10.1016/j.enconman.2019.05.073.
[9] K. Kant, A. Shukla, A. Sharma, Heat transfer studies of building brick containing phase change materials, Sol. Energy 155 (2017) 1233–1242 https://doi.org/, doi:10.1016/j.solener.2017.07.072.
[10] A. Kasaeian, L. bahrami, F. Pourfayaz, E. Khodabandeh, W.M. Yan, Experimental studies on the applications of PCMs and nano-PCMs in buildings: a critical review, Energy Build. 154 (2017) 96–112 https://doi.org/, doi:10.1016/j.enbuild.2017.08.037.
[11] H. Ye, L. Long, H. Zhang, R. Zou, The performance evaluation of shape-stabilized phase change materials in building applications using energy saving index, Appl. Energy 113 (2014) 1118–1126 https://doi.org/, doi:10.1016/j.apenergy.2013.08.067.
[12] N. Zhu, S. Wang, Z. Ma, Y. Sun, Energy performance and optimal control of air-conditioned buildings with envelopes enhanced by phase change materials, Energy Convers. Manag. 52 (2011) 3197–3205 https://doi.org/, doi:10.1016/j.enconman.2011.05.011.
[13] C. Yao, X. Kong, Y. Li, Y. Du, C. Qi, Numerical and experimental research of cold storage for a novel expanded perlite-based shape-stabilized phase change material wallboard used in building, Energy Convers. Manag. (2018) https://doi.org/, doi:10.1016/j.enconman.2017.10.052.

[14] X. Qiao, X. Kong, H. Li, L. Wang, H. Long, Performance and optimization of a novel active solar heating wall coupled with phase change material, J. Clean. Prod. (2020) https://doi.org/, doi:10.1016/j.jclepro.2019.119470.
[15] X. Kong, L. Wang, H. Li, G. Yuan, C. Yao, Experimental study on a novel hybrid system of active composite PCM wall and solar thermal system for clean heating supply in winter, Sol. Energy (2020) https://doi.org/, doi:10.1016/j.solener.2019.11.081.
[16] X. Sun, Q. Zhang, M. a. Medina, K.O. Lee, Energy and economic analysis of a building enclosure outfitted with a phase change material board (PCMB), Energy Convers. Manag. 83 (2014) 73–78 https://doi.org/, doi:10.1016/j.enconman.2014.03.035.
[17] D. Mazzeo, G. Oliveti, A. de Gracia, J. Coma, A. Solé, L.F. Cabeza, Experimental validation of the exact analytical solution to the steady periodic heat transfer problem in a PCM layer, Energy 140 (2017) 1131–1147 https://doi.org/, doi:10.1016/j.energy.2017.08.045.
[18] P. McKenna, W.J.N. Turner, D.P. Finn, Geocooling with integrated PCM thermal energy storage in a commercial building, Energy 144 (2018) 865–876 https://doi.org/, doi:10.1016/j.energy.2017.12.029.
[19] K.O. Lee, M.A. Medina, X. Sun, X. Jin, Thermal performance of phase change materials (PCM)-enhanced cellulose insulation in passive solar residential building walls, Sol. Energy 163 (2018) 113–121 https://doi.org/, doi:10.1016/j.solener.2018.01.086.
[20] F. Souayfane, P.H. Biwole, F. Fardoun, P. Achard, Energy performance and economic analysis of a TIM-PCM wall under different climates, Energy 169 (2019) 1274–1291 https://doi.org/, doi:10.1016/j.energy.2018.12.116.
[21] F. Mehdaoui, M. Hazami, A. Messaouda, H. Taghouti, A.A. Guizani, Thermal testing and numerical simulation of PCM wall integrated inside a test cell on a small scale and subjected to the thermal stresses, Renew. Energy 135 (2019) 597–607 https://doi.org/, doi:10.1016/j.renene.2018.12.029.
[22] X. Jin, M.A. Medina, X. Zhang, On the placement of a phase change material thermal shield within the cavity of buildings walls for heat transfer rate reduction, Energy 73 (2014) 780–786 https://doi.org/, doi:10.1016/j.energy.2014.06.079.
[23] Y. Fang, A Comprehensive Study of Phase Change Materials (PCMs) for Building Walls Applications, University of Kansas, 2009 https://kuscholarworks.ku.edu/handle/1808/5537.
[24] K. Kant, A. Shukla, A. Sharma, P.H. Biwole, P. Henry Biwole, P.H. Biwole, P. Henry Biwole, Heat transfer study of phase change materials with graphene nano particle for thermal energy storage, Sol. Energy 146 (2017) 453–463 https://doi.org/, doi:10.1016/j.solener.2017.03.013.
[25] Rubitherm-RT28HC, Rubitherm Phase Change Materials, Rubitherm. (2018) 40. https://www.rubitherm.eu/media/products/datasheets/Techdata_-RT28HC_EN_06082018.PDF.
[26] Rubitherm-RT-26, Rubitherm Phase Change Material, Rubitherm-RT26. (2018) 30. https://www.rubitherm.eu/media/products/datasheets/Techdata_-RT26_EN_06082018.PDF.
[27] P.H. Biwole, P. Eclache, F. Kuznik, Phase-change materials to improve solar panel's performance, Energy Build. 62 (2013) 59–67 https://doi.org/, doi:10.1016/j.enbuild.2013.02.059.
[28] K. Kant, A. Shukla, A. Sharma, P.H. Biwole, Heat transfer studies of photovoltaic panel coupled with phase change material, Sol. Energy 140 (2016) 151–161 https://doi.org/, doi:10.1016/j.solener.2016.11.006.
[29] K. Kant, A. Shukla, A. Sharma, P.H.P.H. Biwole, Melting and solidification behaviour of phase change materials with cyclic heating and cooling, J. Energy Storage 15 (2018) 274–282 https://doi.org/, doi:10.1016/j.est.2017.12.005.
[30] OMEGA, Emissitivity of Common Materials: Non-Metals Index, (2019). https://www.omega.com/literature/transactions/volume1/emissivityb.html (Accessed 22 February 2019).
[31] RIMAInternational, A Review of Interior Radiation Control Coating Research, 2014. https://www.solec.org/wp-content/uploads/2014/05/A-Review-of-IRCC-Research.pdf.
[32] K. Kant, A. Shukla, A. Sharma, P.H. Biwole, Thermal response of poly-crystalline silicon photovoltaic panels: numerical simulation and experimental study, Sol. Energy 134 (2016) 147–155 https://doi.org/, doi:10.1016/j.solener.2016.05.002.
[33] V.R. Voller, C. Prakash, A fixed grid numerical modelling methodology for convection-diffusion mushy region phase-change problems, Int. J. Heat Mass Transf. 30 (1987) 1709–1719.
[34] A.D. Brent, V.R. Voller, K.J. Reid, Enthalpy-porosity technique for modeling convection-diffusion phase change: application to the melting of a pure metal, Numer. Heat Transf. Part A Appl. 13 (1988) 297–318.
[35] H. Zennouhi, W. Benomar, T. Kousksou, A.A. Msaad, A. Allouhi, M. Mahdaoui, T. El Rhafiki, Effect of inclination angle on the melting process of phase change material, Case Stud. Therm. Eng. 9 (2017) 47–54 https://doi.org/, doi:10.1016/j.csite.2016.11.004.
[36] O. Bertrand, B. Binet, H. Combeau, S. Couturier, Y. Delannoy, D. Gobin, M. Lacroix, P. Le Quéré, M. Médale, J. Mencinger, Melting driven by natural convection A comparison exercise: first results, Int. J. Therm. Sci. 38 (1999) 5–26.
[37] W. Cui, G. Cao, J.H. Park, Q. Ouyang, Y. Zhu, Influence of indoor air temperature on human thermal comfort, motivation and performance, Build. Environ. (2013) https://doi.org/, doi:10.1016/j.buildenv.2013.06.012.
[38] Z.H. Khan, M.R. Islam, R.A. Tarefder, Determining asphalt surface temperature using weather parameters, J. Traffic Transp. Eng. (2019) https://doi.org/, doi:10.1016/j.jtte.2018.04.005.
[39] P.H. Biwole, M. Woloszyn, C. Pompeo, Heat transfers in a double-skin roof ventilated by natural convection in summer time, Energy Build. 40 (2008) 1487–1497 https://doi.org/, doi:10.1016/j.enbuild.2008.02.004.
[40] J. Park, T. Kim, S.-B.B. Leigh, Application of a phase-change material to improve the electrical performance of vertical-building-added photovoltaics considering the annual weather conditions, Sol. Energy 105 (2014) 561–574 https://doi.org/, doi:10.1016/j.solener.2014.04.020.
[41] NSRDB, National Solar Radiation Data Base, Data Sets. (2017). https://rredc.nrel.gov/solar/old_data/nsrdb/; Accessed date, December 2017.